Available online at www.sciencedirect.com
SCIENCE DIRECT®
Journal of Power Sources 132 (2004) 150–155
JOURNAL OF POWER SOURCES
www.elsevier.com/locate/jpowsour

Effect of synthesis method on the electrochemical performance of $LiNi_{1/3}Mn_{1/3}Co_{1/3}O_2$

De-Cheng Li, Takahisa Muta, Lian-Qi Zhang, Masaki Yoshio, Hideyuki Noguchi*

[a] *Department of Applied Chemistry, Saga University, Hohjyo-1, Saga 840-8502, Japan*

Received 15 August 2003; received in revised form 24 December 2003; accepted 5 January 2004

Abstract

$LiNi_{1/3}Mn_{1/3}Co_{1/3}O_2$ was prepared by both the spray dry method and the metal acetate decomposition method. The influences of synthesis method on the electrochemical behaviors of $LiNi_{1/3}Mn_{1/3}Co_{1/3}O_2$ were also characterized. The difference in preparation method results in the difference in compound color, morphology (shape, particle size and specific surface area) and the electrochemical characteristics, such as the shape of first charge curve, reversible capacity and the rate capability. A sample prepared by the spray dry method exhibits an absence of 4.5 V plateau, a higher capacity retention and better rate capability than those prepared by the metal acetate decomposition method. The reversible capacity after 35 cycles is 166 mAh g^{-1} at 50 °C when a cell is cycled at a current density of 0.2 mA cm^{-2} in 3–4.5 V. The operation temperature has little influence on the rate capability of the sample prepared by the spray dry method while pronounced in the case of those samples prepared by the metal acetate decomposition method.

Keywords: Cathode material; $LiNi_{1/3}Mn_{1/3}Co_{1/3}O_2$; Spray dry method; Metal acetate decomposition; Electrochemical behavior

1. Introduction

During the past decade, lithium nickel manganese oxides have been extensively studied as an alternative to $LiCoO_2$, which is the state-of-the-art cathode material in commercial lithium ion battery systems, due to the relative lower cost and toxicity of Ni and Mn compared to Co [1–8]. Recently, much attention has been paid to a layered $LiNi_{0.5}Mn_{0.5}O_2$ that can be considered as a one-to-one mixture of $LiNiO_2$ and $LiMnO_2$ [9–12]. It has many advantages over $LiNiO_2$ and $LiMnO_2$, such as its high capacity, structural and thermal stability, and excellent cyclic performance. Nevertheless, it also has some drawbacks. One is its difficulty in preparation by conventional solid state method, in which Li_2MnO_3 preferentially forms and unreacted NiO remains [13]. Another is its lower electronic conductivity, which dramatically reduces its specific capacity even at a moderate current density [14].

Cobalt doping cannot only promote the formation of $LiNi_{0.5-x}Mn_{0.5-x}Co_{2x}O_2$, but also enhance the electronic conductivity and the thermal stability [15–18]. $LiNi_{1/3}Mn_{1/3}Co_{1/3}O_2$, which can be considered as a compound among $LiNi_{0.5-x}Mn_{0.5-x}Co_{2x}O_2$ series, was first proposed by Ohzuku and Makimura [19]. They initially prepared it by solid state reaction method [19] and re-prepared by mixed hydroxide method [20]. It has a layered structure ($a = 2.862$ Å; $c = 14.227$ Å) with a reversible capacity of more than 200 mAh g^{-1} within the voltage range of 2.5–4.6 V. In addition, it has excellent rate capability and good thermal stability [20]. Chowdari and co-workers also prepared it at 1000 °C by mixed hydroxide method and reported that the predominant oxidation states of Ni, Co, and Mn in the compound were 2+, 3+, and 4+, respectively [21]. However, a closer inspection of their results reveals some contradictory information on the electrochemical behaviors such as the shape of initial charge curve, reversible capacity and cyclic performance. This strongly implied that the electrochemical characteristics of $LiNi_{1/3}Mn_{1/3}Co_{1/3}O_2$ are prone to be affected by preparation condition. In order to further improve its electrochemical performance, it is necessary to study the influence of preparation method on the structural and electrochemical characteristics of $LiNi_{1/3}Mn_{1/3}Co_{1/3}O_2$ and clarify the essential reason of the difference.

The metal acetate decomposition is one of solid state reaction methods by which one can prepare cathode materials for Li-ion batteries [22]. Since the low melting point

* Corresponding author. Tel.: +81-952-28-8674; fax: +81-952-28-8591.
E-mail address: noguchih@cc.saga-u.ac.jp (H. Noguchi).

0378-7753/$ – see front matter © 2004 Elsevier B.V. All rights reserved.
doi:10.1016/j.jpowsour.2004.01.016

of metal acetate, their mixtures would transform to a fluid state when they were exposed to their eutectic temperature. One can, therefore, easily get a well-mixed precursor. The spray dry method is another simple and powerful technique to prepare cathode materials [23,24] by which we can easily get the homogeneous precursors at an atomic level. In the present work, $LiNi_{1/3}Mn_{1/3}Co_{1/3}O_2$ was prepared by both the metal acetate decomposition method and the spray dry method and its structural, morphological and electrochemical behaviors were also characterized.

2. Experimental

2.1. Preparation by the metal acetate decomposition method

Mixtures of stoichiometrical $LiCH_3COO{\cdot}2H_2O$, Ni $(CH_3COO)_2{\cdot}4H_2O$, Mn $(CH_3COO)_2{\cdot}4H_2O$, Co $(CH_3COO)_2{\cdot}4H_2O$ were thoroughly ground and heated at 400 °C to obtain the precursors. Precursor was heated at 900 °C for 20 h in air (sample A). Precursor was initially ball-milled for 1 h and then heated at 900 °C for 20 h in air (sample B). The color of samples A and B is black.

2.2. Preparation by the spray dry method

$LiNO_3$, Ni $(CH_3COO)_2{\cdot}4H_2O$, Mn $(CH_3COO)_2{\cdot}4H_2O$ and Co $(CH_3COO)_2{\cdot}4H_2O$, were dissolved in distilled water to obtain a starting solution. The solution was pumped into Yamato GB32 Pulvis Mini-Spray instrument. Obtained precursor was first heating at 300 °C. After being ground and pressed into pellets, it was sintered at 900 °C for 20 h in air (sample C). Its color is brown, which is difference from those of samples A and B.

The XRD measurement was carried out using a Rigaku Rint1000 diffractometer equipped with a monochromator and Cu target tube.

The scan electron microscope (SEM) study of the samples was performed by JEOL JSM-5200 electron microscope.

The specific surface area for each sample was analyzed by the Brunauer, Emmett, and Teller (BET) method using Micromeritics Gemini2375 in which a N_2 gas adsorption was employed. Each sample was heated to 200 °C for 20 min to remove adsorbed water before measurement.

The charge/discharge tests were carried out using the CR2032 coin-type cell, which consists of a cathode and lithium metal anode separated by a Celgard 2400 porous polypropylene film. The cathode contains a mixture of 20 mg of accurately weighted active materials and 13 mg of the teflonized acetylene black (Table 2) as conducting binder. The mixture was pressed onto a stainless screen and dried at 170 °C for 5 h under vacuum. The cells were assembled in a glove box filled with dried argon gas. The electrolyte is 1 M $LiPF_6$ in ethylene carbonate/dimethyl carbonate (EC/DMC, 1:2 by volume).

3. Results and discussion

Fig. 1 shows the XRD patterns of three $LiNi_{1/3}Mn_{1/3}Co_{1/3}O_2$ samples. All peaks are sharp and well-defined, suggesting that compounds are well crystallized. All peaks of samples B and C can be indexed on the α-$NaFeO_2$ structure (space group: $R\bar{3}m$) while a trace amount of impurity, NiO, was observed in sample A.

The lattice parameters of samples A, B, and C were calculated by a least squares method using 10 diffraction lines and summarized in Table 1. Our samples have smaller lattice parameters, a, c and unit cell volume V while a larger triangle distortion, c/a, and the intensity ratio of I_{003}/I_{104} compared to those reported by Ohzuku and co-workers [19,20]

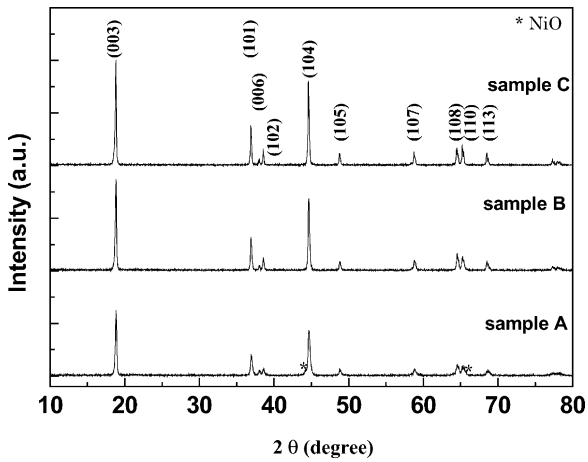

Fig. 1. XRD patterns of $LiNi_{1/3}Mn_{1/3}Co_{1/3}O_2$ prepared by different methods.

Table 1
Lattice parameters of $LiNi_{1/3}Mn_{1/3}Co_{1/3}O_2$ prepared by different methods

Sample	a (Å)	c (Å)	c/a	V (Å^3)	I_{003}/I_{104}
A	2.852	14.208	4.981	100.09	1.25
B	2.854	14.203	4.976	100.21	1.08
C	2.855	14.217	4.979	100.3	1.0
Ohzuku and co-worker's data [19]	2.867	14.246	4.969	101.4	–
[20]	2.862	14.227	4.971	100.6	–
Chowdari and co-worker's data [21]	2.864	14.233	4.969	101.1	0.8

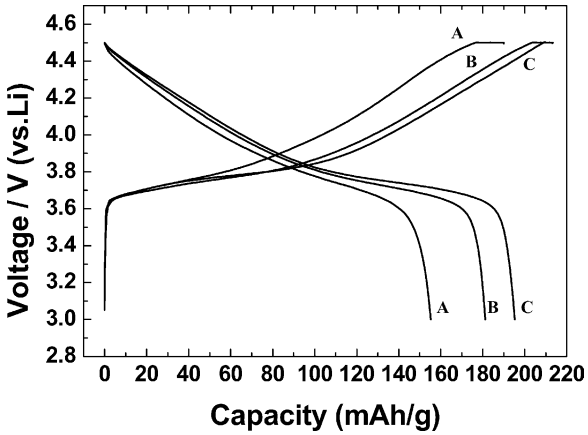

Fig. 2. Initial charge and discharge curves of samples A, B, and C operated at a current density of 0.2 mA cm^{-2} (20 mA g^{-1}) in the voltage of 3–4.5 V.

and Chowdari and co-workers [21]. These differences probably come from the difference in preparation conditions. Since the intensity ratio I_{003}/I_{104} is sensitive to the degree of cation mixing in lattice [25], good electrochemical performance can be expected for our samples. Moreover, gradual change in lattice parameters from A to C implies that sample B is intermediate state between sample A and C. The lattice parameters of sample C are very closed to those reported recently by Yabuuchi and Ohzuku [20].

The initial charge/discharge curves of samples A, B and C were given in Fig. 2. Cells were operated at a current density of 0.2 mA cm^{-2} (20 mA g^{-1}) in the voltage range of 3–4.5 V. The initial charge/discharge capacity at room temperature is 176/155, 203/181, and 208/195 mAh g^{-1} for samples A, B, and C, respectively. Moreover, the electrode composed of sample C shows a lower polarization and irreversible capacity than those of samples A and B. It is interesting to note that there is slight difference among samples A, B, and C in the shape of the charge curve and this difference can be clearly distinguished when cells are operated at 50 °C.

Fig. 3 shows the first charge curves of samples B and C operated at 50 °C. For both of samples, the cell voltage

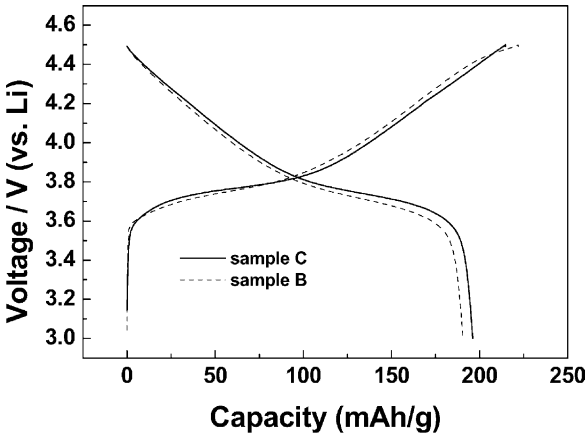

Fig. 3. First charge curves of samples B and C operated at 50 °C.

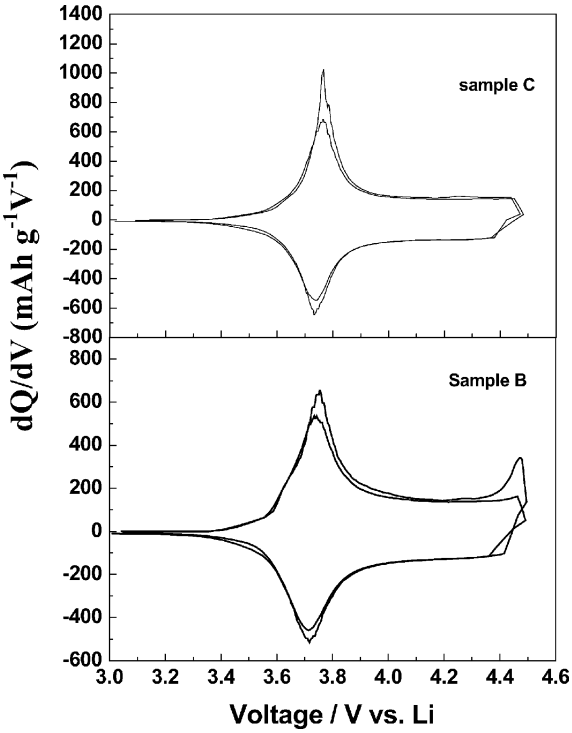

Fig. 4. Differential capacity vs. voltage curves of samples B and C operated at 50 °C.

rapidly increases to about 3.7 V and then holds at 3.7–3.8 V until the charge capacity reaches about 90 mAh g^{-1}. Ohzuku and co-workers [26] reported that oxidation of Ni^{2+} to Ni^{3+} occurred in this region. On further charging, however, the voltage monotonously increases to 4.5 V in the case of sample C while in the case of sample B, it increases at first to 4.4 V almost linearly, and then gradually climbs up to 4.5 V, accompanied a narrow plateau around 4.5 V. This derivation could also be observed if one carefully compared the results of Ohzuku and co-workers [19,20] with the results of Chowdari and co-workers [21].

The differential capacity versus voltage curves of samples B and C operated at 50 °C were given in Fig. 4. Two peaks were observed in case of sample B during the first charge. One is broad and centered at 3.75 V. The other is small and centered at 4.5 V. This small peak is difficult to be distinguished in the following cycle. Chowdari and co-workers [21] have observed the existence of small peak around 4.5 V in the cyclic voltammogram of $LiNi_{1/3}Mn_{1/3}Co_{1/3}O_2$ and assigned it to the Co^{3+}/Co^{4+} redox couple. As the case of sample C, only a sharp peak accompanied by a small shoulder was observed at 3.75 V during the first cycle. In the second cycle, this shoulder peaks emerges into the sharp peak, forming a broaden peak centered at 3.75 V. The origin of this phenomenon is still unclear. Since it is likely to be closely related to the preparation method, we think that its origin is in fact correlated to the true chemical composition of sample. The presence of residual NiO in sample A strongly suggests that they should be considered as a solid

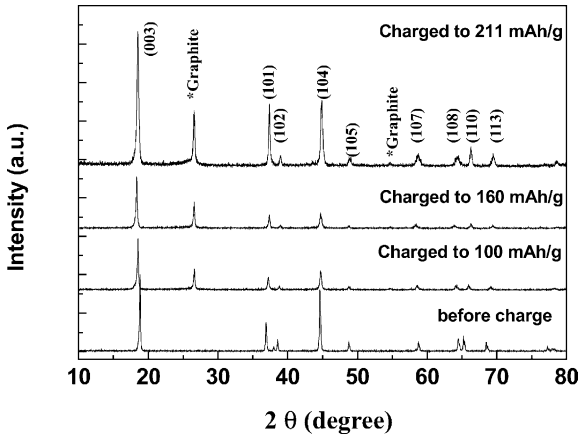

Fig. 5. XRD patterns of charged $LiNi_{1/3}Mn_{1/3}Ti_{1/3}O_2$ composite cathode fabricated with sample C.

solution of a layered compound of Li-Ni-Mn-Co-O with Li_2MnO_3, such as $LiNi_{0.5-x}Mn_{0.5-x}Co_{2x}O_2$–$Li_2MnO_3$ since the plateau around 4.5 V was usually observed in the solid solution of $LiNi_{0.5}Mn_{0.5}O_2$–Li_2MnO_3 (Li $[Ni_xLi_{1/3-2x/3}Mn_{2/3-x/3}]O_2$) [27] and $LiCoO_2$–$LiMn_2O_3$ [28].

Fig. 5 shows the ex-situ XRD patterns of sample C charged up to different capacities. During the charge process, all peaks can also be indexed on the α-$NaFeO_2$ structure. Upon the Li ions removal, the (0 0 3) and the (0 0 6) peaks continuously shift to lower angles while the (1 0 1) and the (1 1 0) peaks shift to high angles, suggesting that Li ions extraction results in the lattice shrinkage along *a*, *b* direction while expansion along *c* direction. These results suggest the layered structure is remained in the range of $x = 0.78$ in $Li_{1-x}Ni_{1/3}Mn_{1/3}Co_{1/3}O_2$ and there is no phase transition between hexagonal and monoclinic, usually observed in $LiCoO_2$ [29] and $LiNiO_2$ [25]. When electrode was charged to 211 mAh g^{-1}, the (1 0 7) and the (1 0 8) peaks shifts to a high value while the (1 1 0) peak shifts to a low value. These results suggest that *c* axis contracts while a axis expands. The broaden (1 0 7) and (1 0 8) peaks imply the existence of strain or defect in lattice caused by Li de-intercalation.

Fig. 6 illustrates the relation between the change in lattice parameters of sample C and the *x*, in $Li_{1-x}Ni_{1/3}Mn_{1/3}Co_{1/3}O_2$. During the charge process, the lattice parameter, *a*, which is related to the average metal–metal intra-slab distance, monotonously reduces at $x \leq 0.6$ and keeps a constant value of ca. 2.82 Å at $0.6 \leq x \leq 0.78$ while the lattice parameter, *c*, which is correlated to the average metal–metal inter-slab distance, increases as *x* increases until *x* reaches the value of about 0.6. This evolution in lattice parameters is commonly observed in layered oxides and can be explained by the decreased ionic radius of oxidized transition metals (Ni, Mn, and/or Co) and the enhancement of electrostatic repulsive force between oxygen ions of two adjacent slabs. Further removal of Li gives rise to the decrease in parameter *c*. The unit cell volume, *V*, however, linearly reduces from 101 Å^3 for $x = 0$ to 99 Å^3 for $x = 0.78$ (about 2% change in volume), which is mainly caused by the shrinkage in a axis. This small change in unit cell volume may give rise to excellent electrochemical performances for our samples.

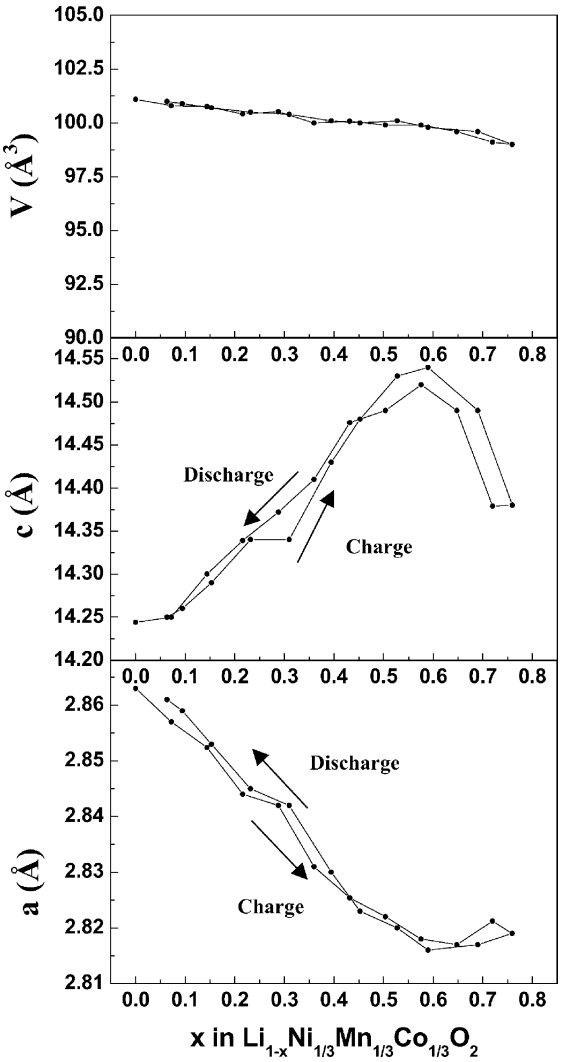

Fig. 6. Relation between the change in lattice parameters of sample C and *x* in $Li_{1-x}Ni_{1/3}Mn_{1/3}Co_{1/3}O_2$.

Fig. 7 shows the rate capabilities of samples B and C operated at room temperature and 50 °C. Cells were at first charged to 4.5 V at a current density of 0.2 mA cm^{-2} (20 mA g^{-1}) and hold at 4.5 V for 3 h (called C.C–C.V mode) then discharged to 3 V at different current densities. The discharge capacity of sample C decreases from 183 mAh g^{-1} at a rate of about 0.1 C (20 mA g^{-1}) to 168 mAh g^{-1} at a rate of about 1.8 C (320 mA g^{-1}) when cells are operated at room temperature. The capacity loss is 15 mAh g^{-1} (about 8% of the discharge capacity at 0.1 C). When cells are cycled at 50 °C, the discharge capacities are 196 mAh g^{-1} (0.1 C) and 186 mAh g^{-1} (1.8 C), respectively.

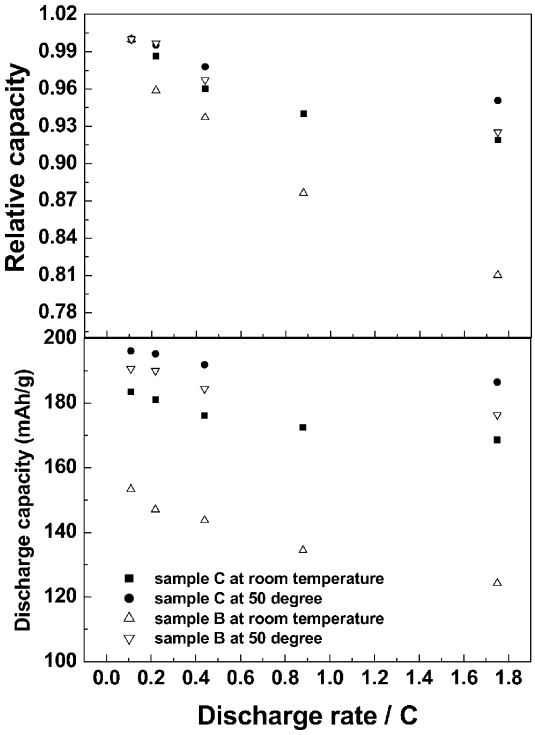

Fig. 7. Rate capabilities of samples B and C operated at room temperature and 50 °C.

About 95% of the discharge capacity at the rate of 0.1 C is available. As for sample B, the decrease in discharge capacity resulting from the discharge current rate increase is 29 mAh g^{-1} (about 20% of the discharge capacity at 0.1 C) at room temperature while 14 mAh g^{-1} (about 8% of the discharge capacity at 0.1 C) at 50 °C. Our results suggest that the rate capability of sample C is slighted influenced by operation temperature whereas the rate capability of sample B is strongly correlated to operation temperature.

Fig. 8 shows the morphologies of samples B and C. Sample B has a well-shaped, smooth of crystals with sharp edges morphology. The particle size ranges from 0.5 to 2 μm. Its specific surface area is ca. 1.9 m^2 g^{-1}. The morphology of sample C is particle-agglomerated, crumbling. The primary particle size is about 0.1 μm. Its specific surface area is ca. 3.4 m^2 g^{-1}, nearly twice as large as that of sample B. Since excellent rate capability have been addressed in Yabuuchi and Ohzuku's results [20], where the charge plateau peak around 4.5 V was no observed in the first cycle, we herein believe that the excellent rate capability of sample C should be related to the absence of impurity (NiO) as well as the smaller particle size with a larger specific surface area.

Fig. 9 shows the cyclic performances of samples A, B, and C cycled at 50 °C. Cells were at first charged to 4.5 V at a current density of 0.2 mA cm^{-2} (20 mA g^{-1}) and hold at 4.5 V for 3 h (called C.C–C.V mode) then discharged to 3 V at a current density of 0.2 mA cm^{-2} (20 mA g^{-1}). All

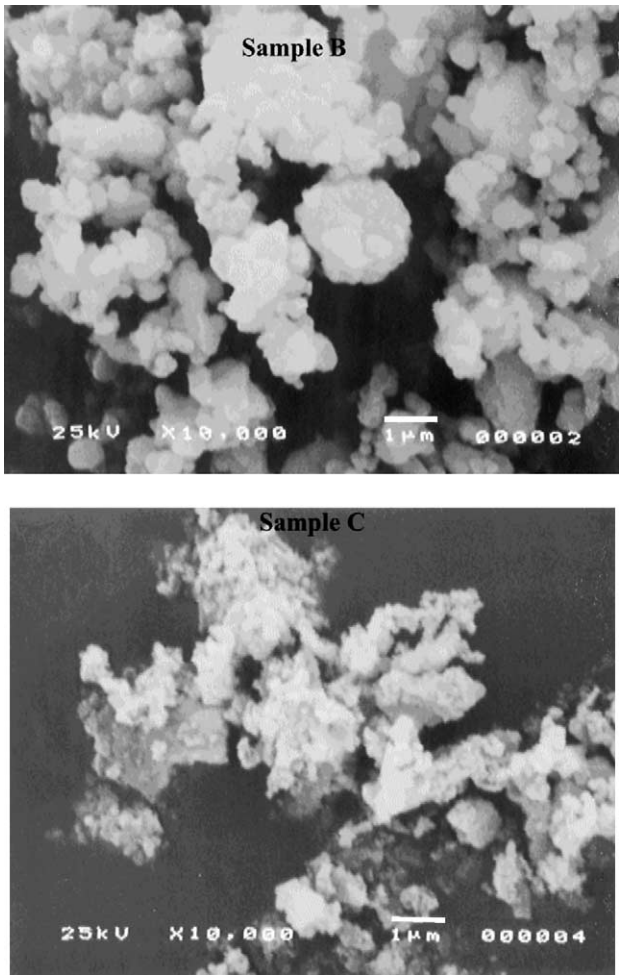

Fig. 8. SEM micrograph of samples B and C.

samples have excellent cyclic performance. The reversible capacity after 35 cycles is 126 mAh g^{-1} (81% of the first discharge capacity), 154 mAh g^{-1} (85% of the first discharge capacity), and 166 mAh g^{-1} (85% of the first discharge capacity) for samples A, B, and C, respectively.

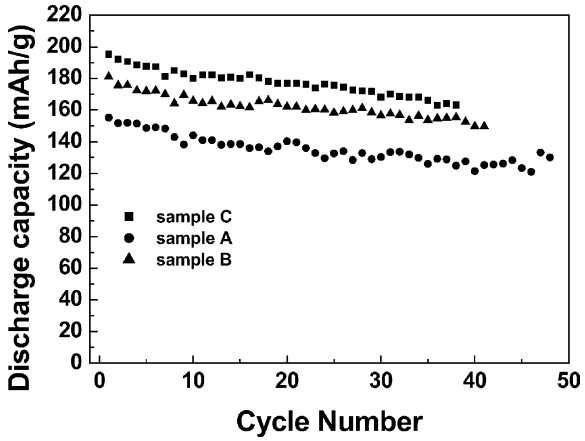

Fig. 9. Cyclic performances of samples A, B, and C cycled at 50 °C.

4. Conclusions

$LiNi_{1/3}Mn_{1/3}Co_{1/3}O_2$ was prepared by both the metal acetate decomposition method and the spray dry method. The difference in preparation method results in the difference in compound color, morphology (shape, particle size and specific surface area) and thereby the difference in the shape of the first charge curve, reversible capacity and the rate capability. Sample prepared by the spray dry method exhibits higher capacity retention, better rate capability than those prepared by the metal acetate decomposition method. Given the presence of unreacted NiO in sample A (also existing in B though it cannot be distinguished from XRD pattern), we would rather regard samples A and B as solid solution systems (for example, a layered compound of Li-Ni-Mn-Co-O with Li_2MnO_3) than pure compound, $LiNi_{1/3}Mn_{1/3}Co_{1/3}O_2$. We believed that the difference in their electrochemical behaviors should be related to the derivation in their chemical composition.

References

[1] E. Rossen, C.D.W. Jones, J.R. Dahn, Solid State Ionics 57 (1992) 311.
[2] Q. Zhong, A. Bonakdarpour, M. Zhang, Y. Gao, J.R. Dahn, J. Electrochem. Soc. 144 (1997) 205.
[3] B.J. Neudecker, R.A. Zuhr, B.S. Kwak, J.B. Bates, J.B. Roberson, J. Electrochem. Soc. 145 (1998) 4148.
[4] M. Yoshio, Y. Todorov, K. Yamato, H. Noguchi, J. Itoh, M. Okada, T. Mouri, J. Power Sources 74 (1998) 46.
[5] J.M. Paulsen, C.L. Thomas, J.R. Dahn, J. Electrochem. Soc. 147 (2000) 861.
[6] Z. Lu, D.D. MacNeil, J.R. Dahn, Electrochem. Solid-State Lett. 4 (2001) A191.
[7] Z. Lu, J.R. Dahn, J. Electrochem. Soc. 149 (2000) A815.
[8] J.-H. Kim, C.S. Yoon, Y.-K. Sun, J. Electrochem. Soc. 150 (2003) A538.
[9] T. Ohzuku, Y. Makimura, Chem. Lett. (2001) 744.
[10] J. Reed, G. Ceder, Electrochem. Solid-State Lett. 5 (2002) A145.
[11] W.-S. Yoon, Y. Paik, X.-Q. Yang, M. Balasubramanian, J. McBreen, C.P. Grey, Electrochem. Solid-State Lett. 5 (2002) A263.
[12] X. Yang, J. McBreen, W. Yoon, C.P. Gray, Electrochem. Commun. 4 (2002) 649.
[13] M. Yoshio, Y. Todorov, K. Yamato, H. Noguchi, J. Itoh, M. Okada, T. Mouri, J. Power Sources 74 (1998) 46.
[14] B.L. Cushing, J.B. Goodenough, Solid State Sci. 4 (2002) 1487.
[15] S.-H. Kang, J. Kim, M.E. Stoll, D. Abraham, Y.K. Sun, K. Amine, J. Power Sources 112 (2002) 41.
[16] Z. Lu, D.D. MacNeil, J.R. Dahn, Electrochem. Solid-State Lett. 4 (2001) A200.
[17] D.D. MacNeil, Z. Lu, J.R. Dahn, J. Electrochem. Soc. 149 (2002) A1332.
[18] D.-Ch. Li, H. Noguchi, M. Yoshio, Electrochim. Acta, submitted for publication.
[19] T. Ohzuku, Y. Makimura, Chem. Lett. 1 (2001) 642.
[20] N. Yabuuchi, T. Ohzuku, J. Power Sources 119 (2003) 171.
[21] K.M. Shaju, G.V. Subba Rao, B.V.R. Chowdari, Electrochim. Acta 48 (2002) 145.
[22] B. Jung, I. Jeong, K. Han, Y. Lee, D. Kim, J. Choo, M. Kim, K. Ryu, Y. Park, E. Kang, J. Jeong, Meeting Abstract of 1st International Conference on Polymer Batteries and Fuel Cell, Tu-072.
[23] J.N. Reimers, E. Rossen, C.D. Jones, J.R. Dahn, Solid State Ionics 61 (1993) 335.
[24] D.-Ch. Li, H. Noguchi, ITE Lett. 4 (2003) 303.
[25] T. Ohzuku, A. Ueda, M. Nagayama, J. Electrochem. Soc. 140 (1993) 1862.
[26] Y. Koyama, I. Tanaka, H. Adachi, Y. Makimura, T. Ohzuku, J. Power Sources 119–121 (2003) 644.
[27] Z. Lu, J.R. Dahn, J. Electrochem. Soc. 149 (2002) A815.
[28] K. Numada, S. Yamanaka, Solid State Ionics 118 (1999) 117.
[29] T. Ohzuku, A. Ueda, J. Electrochem. Soc. 141 (1994) 2972.